Structures of the peptide-modifying radical SAM enzyme SuiB elucidate the basis of substrate recognition

Katherine M. Davis[a], Kelsey R. Schramma[a], William A. Hansen[b], John P. Bacik[a], Sagar D. Khare[b], Mohammad R. Seyedsayamdost[a,c,1], and Nozomi Ando[a,1]

[a]Department of Chemistry, Princeton University, Princeton, NJ 08544; [b]Department of Chemistry and Chemical Biology, Rutgers University, New Brunswick, NJ 08901; and [c]Department of Molecular Biology, Princeton University, Princeton, NJ 08544

Edited by Perry Allen Frey, University of Wisconsin–Madison, Madison, WI, and approved August 18, 2017 (received for review March 3, 2017)

Posttranslational modification of ribosomally synthesized peptides provides an elegant means for the production of biologically active molecules known as RiPPs (ribosomally synthesized and posttranslationally modified peptides). Although the leader sequence of the precursor peptide is often required for turnover, the exact mode of recognition by the modifying enzymes remains unclear for many members of this class of natural products. Here, we have used X-ray crystallography and computational modeling to examine the role of the leader peptide in the biosynthesis of a homolog of streptide, a recently identified peptide natural product with an intramolecular lysine–tryptophan cross-link, which is installed by the radical *S*-adenosylmethionine (SAM) enzyme, StrB. We present crystal structures of SuiB, a close ortholog of StrB, in various forms, including apo SuiB, SAM-bound SuiB, and a complex of SuiB with SAM and its peptide substrate, SuiA. Although the N-terminal domain of SuiB adopts a typical RRE (RiPP recognition element) motif, which has been implicated in precursor peptide recognition, we observe binding of the leader peptide in the catalytic barrel rather than the N-terminal domain. Computational simulations support a mechanism in which the leader peptide guides posttranslational modification by positioning the cross-linking residues of the precursor peptide within the active site. Together the results shed light onto binding of the precursor peptide and the associated conformational changes needed for the formation of the unique carbon–carbon cross-link in the streptide family of natural products.

radical SAM enzyme | SPASM domain | RRE domain | RiPP | streptide

Peptide natural products have had a profound impact on human health as sources of antibacterial, anticancer, and antifungal therapeutics (1, 2). Broadly speaking, they may be synthesized in a ribosome-dependent or -independent manner. The former category comprises the family of ribosomally-synthesized and post-translationally modified peptides (RiPPs). Recent advancements in genome sequencing and bioinformatics have led to the rapid discovery of a multitude of RiPPs and their biosynthetic gene clusters (3). Unlike nonribosomal peptides, which are assembled by large multimodular enzymes (4), RiPP biosynthetic pathways are comparatively simple and thus attractive targets for bioengineering (3). Biosynthesis commences with the ribosomal production of a precursor peptide whose core sequence is modified by tailoring enzymes. Proteolytic removal of the N- and/or C-terminal portions of the peptide, which occurs in most studied cases, followed by export of the mature product, completes RiPP biogenesis. RiPPs encompass structurally and chemically diverse subclasses, such as lanthipeptides, cyanobactins, thiopeptides, and sactipeptides (3). Most recently, a new subclass of RiPPs was identified with the discovery of streptide. It contains an unprecedented lysine–tryptophan carbon–carbon cross-link and is produced by many streptococci (5–7).

Installation of the Lys–Trp cross-link in streptide biosynthesis is catalyzed by the radical *S*-adenosylmethionine (SAM) enzyme StrB (5). Homologs SuiB and AgaB carry out similar reactions (8). As in the production of other RiPPs, streptide biosynthesis requires an N-terminal leader sequence preceding the core peptide sequence (5) (Fig. 1*A*, *Top*). Although such leader sequences are ubiquitous in RiPP precursors, their roles are still under scrutiny. Mounting evidence suggests that the leader sequence directly interacts with the tailoring enzymes to act as a guide that facilitates the modification (9). Recent crystal structures of the lanthipeptide dehydratase NisB and cyanobactin cyclodehydratase LynD have shed light onto leader-sequence recognition by RiPP-tailoring enzymes (10, 11). In both structures, the leader peptide forms an extended β-sheet with a domain that contains a winged helix-turn-helix (wHTH) topology, which was recently classified by HHPred-based bioinformatics as a RiPP precursor peptide recognition element (RRE) (12). Intriguingly, this study further identified the presence of RRE-like domains in the majority of prokaryotic RiPP classes, including those modified by the so-called SPASM-domain containing radical SAM enzymes. Named after founding members subtilosin A, pyrroloquinoline quinone (PQQ), anaerobic sulfatase, and mycofactocin, this subfamily harbors a Cys-rich C-terminal domain that accommodates binding of one or two additional Fe–S clusters. Notably, StrB, AgaB, and SuiB are also members of this subfamily.

Significance

Ribosomally synthesized and posttranslationally modified peptides (RiPPs) are an important class of bioactive natural products. The tailoring enzymes involved in their biogenesis include radical (*S*-adenosylmethionine) SAM metalloenzymes, which often install unusual modifications. The structural basis for substrate recognition in these reactions remains unknown. Herein, we present the X-ray crystal structures of a radical SAM enzyme involved in RiPP biosynthesis. Our structures identify conformational changes correlated with the binding of peptide-substrate and SAM. Surprisingly, we find that the peptide-substrate is not associated with the RiPP recognition element (RRE) but rather observe key contacts to the active site and an important, previously unidentified, bridging domain. These findings reveal unanticipated roles for the RRE and additional domains during RiPP biosynthesis by radical SAM enzymes.

Author contributions: K.M.D., S.D.K., M.R.S., and N.A. designed research; K.M.D., K.R.S., W.A.H., and N.A. performed research; K.M.D., W.A.H., J.P.B., and N.A. analyzed data; and K.M.D., M.R.S., and N.A. wrote the paper.

The authors declare no conflict of interest.

This article is a PNAS Direct Submission.

Data deposition: The atomic coordinates and structure factors have been deposited in the Protein Data Bank, www.wwpdb.org (PDB ID codes 5V1Q, 5V1S, and 5V1T).

[1]To whom correspondence may be addressed. Email: mrseyed@princeton.edu or nozomi.ando@princeton.edu.

This article contains supporting information online at www.pnas.org/lookup/suppl/doi:10.1073/pnas.1703663114/-/DCSupplemental.

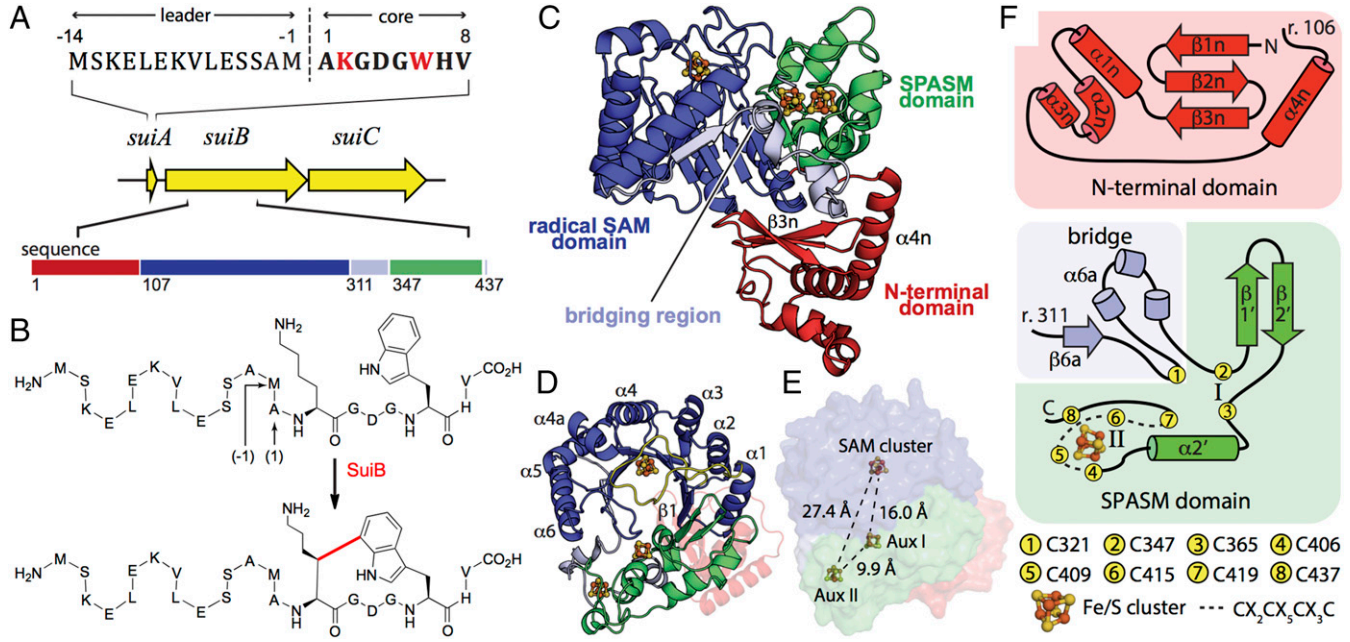

Fig. 1. The *sui* gene cluster and the reaction catalyzed by SuiB. (*A*) The *sui* gene cluster is highly homologous to *str*. It encodes a 22-mer precursor peptide (SuiA), a tailoring radical SAM enzyme (SuiB), and a putative transporter/protease (SuiC). The sequence of SuiA is depicted with the 8-mer sequence of the mature product shown in bold. Cross-linked residues are shown in red. (*B*) SuiB catalyzes Lys–Trp cross-link formation in SuiA. The new bond installed is shown in red. (*C*) SuiB contains three [4Fe–4S] clusters and multiple functional domains. (*D*) The radical SAM domain (blue) forms a partial TIM barrel that is laterally closed by the auxiliary cluster-containing SPASM domain (green). The canonical catalytic [4Fe–4S] cluster-binding motif following β1 is shown in yellow. The bridging region and N-terminal domains are shown in light blue and red, respectively. (*E*) Placement of the three [4Fe–4S] clusters, shown in ball and stick representation (Fe, orange; S, yellow). Distances are calculated between the nearest atoms. (*F*) Topologies of the N-terminal domain, SPASM domain, and bridging region.

Radical SAM enzymes reductively cleave SAM bound to a $[4Fe\text{-}4S]^{+}$ cluster to generate a 5′-deoxyadenosyl radical (5′-dA·), which initiates turnover by abstraction of a hydrogen atom from the substrate (13, 14). In the biosynthesis of streptide and its homologs, hydrogen atom abstraction occurs from the lysine β-hydrogen in the precursor peptide (5, 8). The resultant lysyl radical then reacts with the tryptophan side chain to create a cross-link (Fig. 1*B*). Like other members of the SPASM subfamily, StrB, AgaB, and SuiB, which install Lys–Trp cross-links in their respective peptides, also contain a C-terminal domain with a characteristic 7-cysteine motif ($CX_{9-15}GX_4C$–gap–$CX_2CX_5CX_3C$–gap–C), which allows for binding of additional, so-called "auxiliary" [4Fe–4S] clusters (15). Although this motif has been shown to be necessary for streptide biosynthesis (5), the precise role of auxiliary clusters in SPASM enzymes remains an active area of investigation (16–18).

Here, we report crystal structures of SuiB and thus a visualization of a RiPP-modifying radical SAM enzyme. Using X-ray diffraction, we determined three structures that illustrate conformational changes associated with binding of SAM and substrate SuiA. These structures depict an N-terminal RRE domain positioned at the entrance to the active site that appears poised to support precursor binding. Surprisingly, however, we detect little interaction between the RRE domain and SuiA and instead observe an α-helical peptide corresponding to the leader sequence of SuiA bound within the catalytic barrel formed by the radical SAM and SPASM domains. We identify specific hydrogen-bonding interactions made by a region of the barrel that is stabilized by an auxiliary [4Fe–4S] cluster and a highly conserved amino acid motif (LESS) within the SuiA leader sequence. Using computational methods, we further demonstrate that binding of the leader sequence within the catalytic barrel facilitates conformations that position the core sequence within the active site, bringing the cross-linking residues in proximity of the 5′-carbon of 5′-dA. Together, these results provide structural insights into binding of the precursor peptide to SuiB and the conformational changes needed for the unprecedented C–C cyclization reaction.

Results

Overall Structure of SuiB. SuiB is encoded by *Streptococcus suis* and is 96% homologous to the enzyme StrB from *Streptococcus thermophilus*. Both enzymes install Lys–Trp cross-links in their respective substrates, SuiA and StrA (5, 8). Purification and reductive reconstitution of N-terminally His_6-tagged SuiB leads to an average Fe/S content of 10.4 ± 0.1 Fe and 9.0 ± 0.1 S per protomer. To visualize the overall architecture of SuiB and the conformational changes associated with substrate binding, we determined three crystal structures (*SI Appendix*, Tables S1 and S2). A substrate-free crystal structure of SuiB was determined to 2.5-Å resolution. Additionally, crystals were soaked with excess SAM to yield a structure of SAM-bound SuiB to 2.5-Å resolution. The highest resolution structure at 2.1 Å was solved for reconstituted SuiB cocrystallized with excess SAM and precursor peptide SuiA. Crystals did not form in the presence of peptide alone.

The overall structure of SuiB contains three functionally distinct domains (Fig. 1*C*), described in detail below: the N-terminal RRE domain (residues 1–106), the radical SAM domain (residues 107–310) followed by a short bridging region (residues 311–346), and the C-terminal SPASM domain (residues 347–437).

SuiB Contains a Canonical Radical SAM Domain. The catalytic core of SuiB (residues 107–439) forms a hollow barrel composed of the radical SAM domain bridged to the C-terminal SPASM domain. Characteristic to many members of the radical SAM superfamily, the SAM domain consists of a partial $(\beta/\alpha)_6$ triose phosphate isomerase (TIM) barrel (Fig. 1*D*, blue) that houses the active site [4Fe–4S] cluster in a loop immediately after the β1 strand (13, 19). Contained within this loop (Fig. 1*D*, yellow), Cys117, Cys121, and Cys124 form the so-called radical SAM $CX_3CX\Phi C$ motif (in which Φ is an aromatic residue) and ligate three of the four irons in the SAM cluster. As expected, our substrate-free structure has an open coordination site at the remaining "unique Fe," whereas in our SAM-soaked structure, we observe intact SAM forming a

chelate at this position (*SI Appendix*, Fig. S1). Additional structural motifs critical for SAM binding are also conserved in SuiB (*SI Appendix*), such as hydrogen bonding between the main-chain carbonyl oxygen of the hydrophobic residue Φ (Phe123) and the N6-amino group of adenine (19) (*SI Appendix*, Fig. S1). Although a canonical TIM barrel is composed of eight strands and eight helices, the entire fold has rarely been observed among radical SAM enzymes (13, 19). Instead, the C-terminal SPASM domain provides a lateral closure in SuiB (16, 17, 20) (Fig. 1*D*, green).

The Bridging Region Provides a Critical Residue for Auxiliary Cluster Ligation. Previous biochemical analyses with StrB and SuiB have not unambiguously determined the number of auxiliary clusters. Our structures clearly reveal two intact auxiliary [4Fe–4S] clusters (Fig. 1*E*), similar to anSMEcpe, the anaerobic sulfatase maturating enzyme from *Clostridium perfringens* and the only other structurally characterized member of the SPASM subfamily (17). Full ligation of two auxiliary clusters in SuiB is enabled by an eighth anterior cysteine (Cys321) within the bridging region. This cysteine is located much farther upstream compared with previously characterized SPASM enzymes, at a position 26 residues before the 7-cysteine motif (Fig. 1*F*, light blue). Following the C terminus of the radical SAM domain, the β6a strand of the bridging region dips into the barrel to provide this initial coordinating residue for the first auxiliary cluster, Aux I, before exiting the barrel as a fragmented helix (Fig. 1 *C* and *F*). Although the presence of a cysteine within the bridging region appears to be common to many SPASM radical SAM enzymes (15–17, 20, 21), the large gap in sequence appears to be unique to characterized members within this subfamily and a key feature of Lys–Trp cross-linking enzymes (5).

The SPASM Domain Binds Two Fe–S Clusters. The SPASM domain incorporates the auxiliary clusters around a β-hairpin and α-helix. It is initiated by two cysteines, Cys347 and Cys365, which, in addition to Cys-321, ligate Aux I and flank the β-hairpin. The first strand of the SPASM motif (β1′) interacts with β1 of the radical SAM domain to extend the β-sheet within the barrel (Fig. 1 *D* and *F*). Following residue Cys365, the 7-cysteine SPASM motif is punctuated by the α2′ helix and resumes with the remaining $CX_2CX_5CX_3C$ sequence. The first three cysteines in this sequence—Cys406, Cys409, and Cys415—encircle and ligate the second auxiliary cluster, Aux II, before the chain hooks back to provide the final coordinating residue for Aux I, Cys419. The SuiB sequence then doubles back again to fully coordinate Aux II with the final cysteine of the SPASM motif, Cys437, after which it terminates at Leu439, in contrast to the extended C-terminal helix (α6′) observed in anSMEcpe (17) (Fig. 1*F* and *SI Appendix*, Fig. S2). Aux I and II are located 16.0 Å and 27.4 Å from the radical SAM cluster, respectively, measured between the closest atoms (Fig. 1*E*). As in anSMEs, full cysteine ligation precludes a substrate-binding role for the auxiliary clusters, a conclusion that is further supported by the SuiA-bound structure described below.

The N-Terminal Domain Adopts an RRE Fold. As predicted by previous bioinformatics studies (12), the N-terminal domain of SuiB shows structural homology with the archetypal RRE domain, PqqD (22, 23). Although PqqD is believed to act as a peptide chaperone for PqqE, the radical SAM enzyme involved in PQQ biosynthesis, these two proteins have never been visualized in complex (24–26). Our structures thus provide insight into the arrangement of an RRE-like domain associated with a radical SAM enzyme. The RRE domain in SuiB is initiated by a three-stranded antiparallel β-sheet that adjoins a trihelical bundle (Fig. 1*F*, red), forming a wHTH-like motif that protrudes from the catalytic core (27) (Fig. 1*C*, red). This domain is then anchored in a cleft formed between the SPASM domain (Fig. 1*C*, green) and adjacent bridging region (Fig. 1*C*, light blue) via an additional helix $\alpha4_n$ (Fig. 1*C* and *SI Appendix*, Fig. S3), placing the β-sheet of the wHTH motif above the TIM barrel entrance. In the recent structures of NisB and LynD, the leader peptides are observed in between $\alpha3_n$ and $\beta3_n$, forming an extended antiparallel β-sheet with the wHTH motif (10, 11) (*SI Appendix*, Fig. S3). Differences in sequence between SuiB and its close homologs are also concentrated in this groove (*SI Appendix*, Fig. S4).

Recognition of the Leader Sequence by the Catalytic Core. The enzyme crystallized in the presence of SAM and SuiA yields clear density for the leader portion of the substrate peptide (residues −13 to −1) (Fig. 2*A*), while density for the core sequence (residues 1–8) is disjointed and difficult to assign. In contrast to the structures of NisB and LynD, where the RRE domains make many direct interactions with the respective substrates (10, 11) (*SI Appendix*, Fig. S3), we observe the leader sequence of SuiA bound within the SuiB barrel, adjacent to both the bridging region, which provides the first cysteine ligand for Aux I, and the SPASM domain (Fig. 2*B*). Furthermore, the α-helical nature of the SuiA leader, predicted from sequence analysis, is maintained within the catalytic barrel before it transitions into a loop, whose contiguous density terminates immediately before the core sequence, adjacent to Aux I (Fig. 2*C*). While many RiPP leader peptides have been shown to adopt α-helical conformations in trifluoroethanol, the persistence of this secondary structure upon binding to the tailoring enzyme has only been observed in our structures and the recent structure of MdnC, which binds the leader peptide as a single-turn α-helix but lacks sequence homology to a typical RRE (3, 9, 11, 28).

Recognition of the SuiA leader sequence is primarily achieved through interactions with the bridging region (Fig. 2*C*). These interactions orient the substrate helix and thereby facilitate proper arrangement of the core sequence in the active site (Fig. 2*C* and *SI Appendix*, Fig. S5). Perhaps explaining its high conservation in

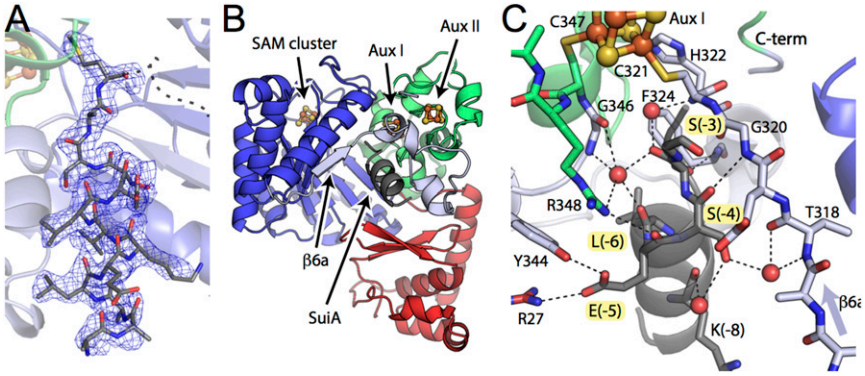

Fig. 2. SuiA recognition in the active site is dominated by interactions of the leader sequence with the bridging region. (*A*) Observed electron density for the helical leader sequence displayed as a $2F_O$-F_C composite omit map contoured at 1.0 σ. The disordered core sequence is represented by a dashed line. (*B*) SuiA (dark gray) binds in the catalytic barrel rather than to the putative recognition element, the N-terminal domain (red). (*C*) Hydrogen-bonding network of SuiA (dark gray) bound in the active site adjacent to the bridging region (light blue) and SPASM domain (green). Ordered water molecules are shown as red spheres. The LESS motif is highlighted. See *SI Appendix*, Fig. S5*A* for a stereoview.

streptide precursor peptides (5), the LESS motif of the leader sequence (residues −6 to −3) plays a particularly important role in orienting SuiA by providing the only hydrogen-bonding partners with SuiB. This hydrogen-bonding network is initiated by water-mediated interactions between SuiA-Leu(−6) and Gly346 in the bridging region and by Arg348 in the SPASM domain (Fig. 2*C* and *SI Appendix*, Fig. S5). The SPASM domain further hydrogen bonds with the backbone carbonyl oxygens of both SuiA-Glu(−5) and, indirectly, SuiA-Ser(−3) through Arg348. The only observed interaction with the RRE motif is made between SuiA-Glu(−5) and Arg27 in the form of a salt bridge. The remaining interactions occur with the bridging region and include Tyr344/SuiA-Glu(−5), Gly320/SuiA-Ser(−4), Phe324/SuiA-Ser(−3), and indirect water-mediated interactions with Thr318, His322, and Gly346 (Fig. 2*C* and *SI Appendix*, Fig. S5). The buried surface area along the peptide–protein interface spanning from the barrel opening to the active site is 730 Å^2, almost 51% of the modeled peptide's total surface area.

Substrate Binding Is Coupled to Loop Movements. The three snapshots obtained in this study illustrate the conformational changes associated with substrate binding by SuiB. Comparison of the substrate-free and SAM-soaked structures shows minimal conformational changes associated with binding of SAM alone (average Cα rmsd of 0.285 ± 0.037 Å) (Fig. 3*A*, gray curve). In the absence of peptide, we observe density for intact SAM bound in the active site, suggestive of a preturnover state (*SI Appendix*, Fig. S1). Crystallization with SAM and SuiA results in large-scale rearrangements (Fig. 3*A*, red/blue curves). At the bottom of the barrel, as oriented in Fig. 1*C*, the largest changes are seen in the RRE-like domain and the α6 helix, which are angled farther away from the barrel opening upon binding of SuiA (Fig. 3*A* and *SI Appendix*, Fig. S6 *A* and *B*). These regions make a number of crystal lattice contacts, making further interpretation difficult; however, it is evident that the enzyme can accommodate significant motions, particularly in the RRE domain. In contrast, motion at the top of the barrel is unencumbered by crystal contacts and is dominated by two loops, L1 and L2, linked by hydrogen-bonding interactions between the backbone carbonyl of Gly122 and backbone amides of Lys286 and Ile287 (Fig. 3*B* and *SI Appendix*, Fig. S6*C*). In particular, residues 125–134 of L1 and 279–285 of L2 adopt a new conformation in the SuiA-bound structure, which occludes the active site. Interestingly, L1 directly follows the SAM-cluster binding motif, and its displacement is likely a result of SAM cleavage in the active site.

A Postturnover Conformation in SuiA-Bound Structure. In our SuiA-bound structure, we observe two disconnected regions of density in close proximity to the SAM cluster (*SI Appendix*, Fig. S1). The first supports Met bound as a tridentate chelate to the unique Fe through its α-amine, carboxylate, and side-chain sulfur atom, an arrangement that mirrors previously observed post-SAM cleavage structures (29–31). This is consistent with prereduction of SuiB with sodium dithionite before crystallization (8). Surprisingly, however, 5′-dA cannot completely account for the second region of density. Instead, we observe intact SAM at this position (*SI Appendix*, Fig. S1). In the absence of a suitable reductant, this unusual feature possibly occurred following a single turnover, in which dynamic motion of the enzyme trapped excess SAM in the active site, perhaps poised to replace the Met bound on the SAM cluster in preparation for another catalytic cycle.

The active-site hydrogen-bonding arrangement persists in the SuiA-bound and SAM-bound structures, with additional hydrogen bonds observed from Glu319 and Arg272 to the methionine moiety of the trapped SAM (13, 19) (*SI Appendix*, Fig. S1). Further analysis of the 5′-dA portion of SAM shows that the 5′-C of the ribose group tilts down toward the peptide substrate, priming the enzyme for H-atom abstraction. This arrangement of the 5′-dA moiety of SAM mimics previously observed SAM-cleavage products in other radical SAM enzymes (29–31) (Fig. 4*A*). Together, these observations suggest that SuiB in complex with SuiA is trapped in a post-SAM cleavage conformation.

Consistent with this post-SAM cleavage model are the shifts observed in L1 upon SuiA binding. The adenine and ribose moieties of SAM make all of the previously observed contacts observed for the 5′-dA moiety in the SAM-only structure. As in the SPASM-containing enzymes anSMEcpe (17) and sporulation-killing factor maturase SkfB (32), as well as the partial-SPASM enzyme 2-deoxy-scyllo-inosamine dehydrogenase BtrN (16), an additional aromatic residue directly follows the final cysteine of the radical SAM motif. In SuiB, this residue is Phe125 (*SI Appendix*, Fig. S2). While the position of the adenine moiety is virtually unchanged between structures, L1 shifts to create an additional hydrogen bond between the backbone of Phe125 and the N7 position of adenine (*SI Appendix*, Fig. S1). Concurrently, the Phe125 side chain flips to stack perpendicularly with the nucleobase, creating a hydrophobic pocket that likely would facilitate stabilization of the cleaved products (*SI Appendix*, Fig. S1*F*).

Coupled together through hydrogen-bonding interactions, changes in L1 result in coordinated rearrangement of L2. Furthermore, movement of Phe125 generates an additional interaction between its backbone carbonyl group and the side chain of Thr282 (L2) (*SI Appendix*, Fig. S6*C*). As a result, the residues of L2 move together to cap the barrel (Fig. 3*B*), perhaps also inducing significant motion in the downstream α6 helix. A comparison of surface renderings, with and without peptide bound, visually confirms constriction of the channel supplying bulk-solvent access to the active site from the top of the barrel (*SI Appendix*, Fig. S6*B*). It is possible that, by limiting solvent access, L2 facilitates a dielectric change in the active site, which has previously been proposed to lower the free-energy barrier for SAM cleavage (33). Intriguingly, an associated channel also connects Aux I to SuiA, suggesting that loop motions may be important for redox reactions involving Aux I.

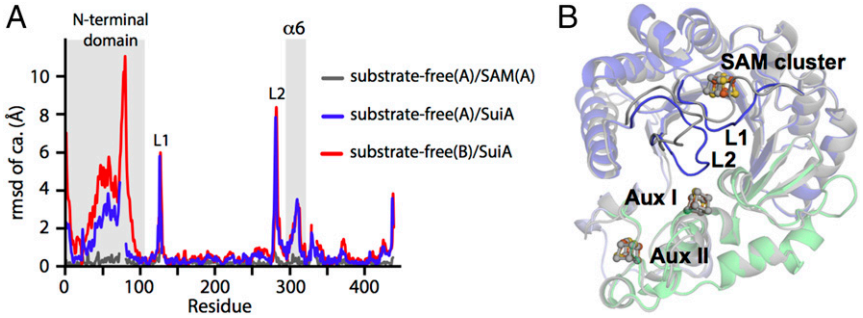

Fig. 3. Substrate binding leads to coordinated loop movements. (*A*) Rmsd of the Cα atoms versus residue number upon SAM and SAM + SuiA binding, respectively. The two chains (*A*/*B*) in the asymmetric unit are denoted parenthetically. Binding only SAM leads to minimal changes (gray curve), yielding an average Cα rmsd of 0.285 ± 0.037 Å, whereas additional binding of SuiA leads to greater changes (blue/red), particularly in the loops L1 and L2. See *SI Appendix*, Fig. S6 for additional views. (*B*) Visualization of loop motions upon SuiA binding. The substrate-free enzyme is shown in gray. The RRE is omitted for clarity.

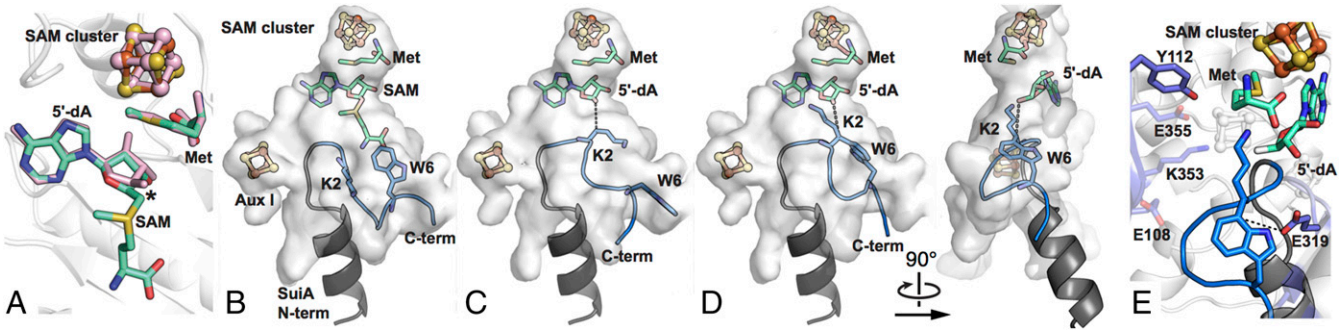

Fig. 4. Binding of the SuiA leader sequence supports positioning of the core sequence in the active site of SuiB. (*A*) The arrangement of Met and SAM (green) in our SuiA-bound structure mimics previously observed SAM-cleavage products from RlmN (pink) (29–31). The 5′-C of 5′-dA is marked with an asterisk. (*B–D*) The active-site cavity of SuiB is shown as a white surface. The crystallographic model of the leader peptide is shown in gray. Rosetta-based simulations yield low-energy conformations of the core sequence (blue) within our SuiA-bound crystal structure both with (*B*) intact SAM and (*C*) the methionine moiety of SAM removed. (*D*) Simulations also yield low-energy conformations of the cyclized core peptide (blue) within the active-site cavity. (*E*) Of the five titratable residues (shown as sticks) near the active site, simulations favor E319 (~4.9 Å from the SuiA-W6 C7 position) as the catalytic base.

The Leader Sequence Helps Position the Core Sequence. The final eight residues of SuiA are disordered in our crystal structure. To investigate the possible conformations adopted by these eight residues within the SuiA-bound crystal structure, two Rosetta-based simulations were performed: one with the Lys–Trp-cyclized SuiA and a second with the linear SuiA substrate. First, the cyclized SuiA core peptide was modeled using NMR-derived constraints for streptide (5) and placed in the active site of the SuiA-bound structure using geometric constraints imposed by a peptide bond linkage to the crystallographic model of the leader peptide. This simulation led to SuiA placements showing considerable steric clashes with the methionine moiety of SAM, which occupies the 5′-dA site. We next modeled uncyclized SuiA in the active site of our SuiA-bound structure. This simulation yielded multiple low-energy conformations of SuiA compatible with the crystallographic model of SuiB (Fig. 4*B*, modeled region of SuiA shown in blue) displaying conformational heterogeneity (Cα rmsds of up to 3.4 Å) that may explain the observed lack of resolvable electron density in our crystal structure.

As the adenine and ribose moieties of SAM in our SuiA-bound structure mimic the postcleavage conformation of 5′-dA (29–31) (Fig. 4*A*), two additional simulations were performed to model the final eight SuiA residues within our SuiA-bound structure with the methionine moiety of SAM removed. Eleven residues lining the barrel, including those that form hydrogen bonds with the methionine moiety of SAM, were allowed to sample other side-chain conformations (*SI Appendix*). Cβ of SuiA-K2 was additionally constrained to within reasonable hydrogen abstraction distances (2.8–4.3 Å) from the adenosine 5′-C (Fig. 4 *C* and *D*, dotted line). Modeling uncyclized SuiA led to multiple low-energy conformations (Fig. 4*C*, modeled region of SuiA shown in blue), suggesting that the leader sequence can facilitate correct positioning of the substrate. In the final simulation, cyclized SuiA was modeled into the active site (Fig. 4*D*, modeled region of SuiA shown in blue). Four clusters of low-energy conformations were observed, displaying relatively high backbone similarity (*SI Appendix*, Figs. S7 and S8). Of the 11 SuiB residues allowed to sample other side-chain conformations, Gln26, Glu108, and Asn315 adopt a conformation not seen in the crystal structure, while Glu319 and Arg272 adopt multiple conformations, including those seen in the structure. Notably, Glu319 and Arg272, which interact with the methionine moiety of SAM in the SuiA-bound structure (*SI Appendix*, Fig. S1*D*), form new interactions with the substrate peptide in these simulated models. In all of these conformations, Glu319 is the closest residue to C7 of SuiA-W6 (within ~5 Å) (Fig. 4*E*). Overall, these simulations are consistent with a scenario in which the SuiA leader sequence positions the core sequence into the active site of SuiB for posttranslational modification.

Discussion

In addition to exploring the conformational changes that facilitate Lys–Trp cross-link formation, the crystal structures presented here provide insights into the functions of ancillary domains that are prevalent in the radical SAM enzyme superfamily. As expected from bioinformatic analyses, the N-terminal domain in SuiB adopts a RRE fold that is docked at the opening of the radical SAM catalytic core, poised to mediate peptide delivery. However, rather than binding to the RRE domain, we observe the SuiA leader peptide primarily interacting with the catalytic barrel. Unique among published RRE-containing structures, this discovery not only elucidates leader peptide function but also provides insights into the role of the RRE domain during catalysis. Simulations of the core sequence further support the role of the leader peptide in guiding posttranslational modifications, while the observed interactions between SuiA and SuiB highlight the importance of a bridging loop linking the radical SAM and SPASM domains. As only the second crystallographically characterized radical SAM enzyme to contain three [4Fe–4S] clusters, SuiB provides additional insights into the SPASM domain and the RRE domain and highlights the unsuspected importance of the bridging domain during catalysis (34).

While more than a third of SPASM-containing enzymes include a cysteine in the bridging region (35), the prevalence of fully ligated auxiliary clusters is unknown. Coordination of the upstream cysteine in SuiB precludes direct substrate binding and establishes this feature, first observed in anSMEcpe, as a significant auxiliary cluster-binding motif. There are, however, critical differences between SuiB and anSMEcpe, including the remote position of the upstream cysteine and fragmentation of the α6a helix (*SI Appendix*, Fig. S9). In addition, the arrangement of the bridging region is indicative of a structural role for Aux I that is further supported by mutagenesis studies, in which C347A/C365A mutants are recalcitrant to purification (8). This region further provides critical contacts for both SuiA and the peptidyl substrate surrogates of anSMEcpe and likely serves a similar binding role in other SPASM-containing enzymes. Thus, variability in the bridging region from one enzyme to another may indicate adaption to the cognate peptide substrate.

Although structural insights remain scarce (10, 11, 23, 36, 37), recent bioinformatic identification of an RRE motif across all RiPP classes has provided invaluable clues to understanding interactions between RiPP precursor peptides and tailoring enzymes. Supported by structural and biochemical analyses, this domain has been implicated in peptide recognition and recruitment. Intriguingly, the structures of SuiB provide an example of a precursor binding location distinct from the RRE domain. This unique SuiA-binding mode suggests that

the RRE-like domain in SuiB is either vestigial or involved in an undetected interaction. Observed motion of the N-terminal domain appears to support the latter, and one can envision a simple scenario in which the RRE both recognizes the peptide and delivers it to the active site but at a certain stage in the catalytic cycle releases the precursor peptide. Recent biochemical analysis of the PqqD/PqqE system not only detected peptide binding to the canonical RRE but also confirmed interaction between the peptide chaperone and radical SAM enzyme. Perhaps the RRE domain in SuiB serves as a similar intermediate binding site (12).

The observed location of SuiA within the barrel may provide insights into mechanism of SuiB. In the catalytic scheme proposed, an active site base facilitates rearomatization by deprotonating the putative tryptophanyl radical intermediate followed by electron transfer to an auxiliary cluster (5). Inspection of the barrel interior yields five possible titratable side chains within ∼10 Å of the adenosine 5′-carbon: Glu319, Glu108, Glu355, Tyr112, and Lys353 (Fig. 4*E*). The positions of simulated Lys–Trp cross-link conformations, supported by alignments with substrate-bound structures of anSMEcpe and RlmN (*SI Appendix*, Fig. S10), favor Glu319 for direct active-site deprotonation (Fig. 4*E*). In this step of the catalytic cycle, Aux II is clearly an unsuitable direct electron acceptor, as it is too far removed from the active site. Electron transfer likely proceeds to Aux I first. Decreased access to bulk solvent as a function of loop movements could then justify electron transfer from Aux I to Aux II and then to a protein redox partner (38).

In conclusion, we present a sequence of structures that not only helps to elucidate the formation of a streptide C–C cross-link but also provides insights into the interplay between RiPP precursor peptides and tailoring enzymes more generally. The structures presented here further demonstrate that the mode of substrate binding greatly contributes to structural diversity within ancillary domains of the radical SAM superfamily. In particular, we gain a newfound appreciation for the bridging region between the SAM and SPASM domains. It will be fascinating to see if future investigations into peptide recognition and recruitment by RiPP-modifying enzymes uncover similar interactions between distinct RRE and catalytic domains, especially those involving radical SAM enzymes like the PqqD/PqqE system.

Materials and Methods

Detailed descriptions of materials and methods, including purification and crystallization of SuiB in various forms, acquisition of X-ray diffraction data, structural elucidation of SuiB and refinement, as well as Rosetta-based calculations, are given in *SI Appendix*.

ACKNOWLEDGMENTS. We thank Dr. Phil Jeffrey at the Princeton Macromolecular Crystallography Facility for invaluable advice on structure refinement and Dr. Steve Meisburger, Saad Imran, and Will Thomas for assistance with X-ray data collection. Diffraction data were collected at the Cornell High Energy Synchrotron Source (CHESS) A1 Station and 23-ID-B of the Advanced Photon Source (APS). CHESS is supported by NSF Grant DMR-1332208, and the MacCHESS facility is supported by NIH NIGMS Grant GM-103485. APS is a US Department of Energy (DOE) Office of Science User Facility operated for the DOE Office of Science by Argonne National Laboratory under Contract DE-AC02-06CH11357, and GM/CA@APS is supported by funds from NIH NCI Grant ACB-12002 and NIGMS Grant AGM-12006. This work was supported by NIH Grants GM098299 (to M.R.S.) and GM100008 (to N.A.), the Arnold O. Beckman Postdoctoral Fellowship program (K.M.D.), and start-up funds from Princeton University (to M.R.S. and N.A.).

1. Ortega MA, van der Donk WA (2016) New insights into the biosynthetic logic of ribosomally synthesized and post-translationally modified peptide natural products. *Cell Chem Biol* 23:31–44.
2. Felnagle EA, et al. (2008) Nonribosomal peptide synthetases involved in the production of medically relevant natural products. *Mol Pharm* 5:191–211.
3. Arnison PG, et al. (2013) Ribosomally synthesized and post-translationally modified peptide natural products: Overview and recommendations for a universal nomenclature. *Nat Prod Rep* 30:108–160.
4. Finking R, Marahiel MA (2004) Biosynthesis of nonribosomal peptides1. *Annu Rev Microbiol* 58:453–488.
5. Schramma KR, Bushin LB, Seyedsayamdost MR (2015) Structure and biosynthesis of a macrocyclic peptide containing an unprecedented lysine-to-tryptophan crosslink. *Nat Chem* 7:431–437.
6. Fleuchot B, et al. (2011) Rgg proteins associated with internalized small hydrophobic peptides: A new quorum-sensing mechanism in streptococci. *Mol Microbiol* 80:1102–1119.
7. Ibrahim M, et al. (2007) Control of the transcription of a short gene encoding a cyclic peptide in Streptococcus thermophilus: A new quorum-sensing system? *J Bacteriol* 189:8844–8854.
8. Schramma KR, Seyedsayamdost MR (2017) Lysine-tryptophan-crosslinked peptides produced by radical SAM enzymes in pathogenic streptococci. *ACS Chem Biol* 12:922–927.
9. Oman TJ, van der Donk WA (2010) Follow the leader: The use of leader peptides to guide natural product biosynthesis. *Nat Chem Biol* 6:9–18.
10. Koehnke J, et al. (2015) Structural analysis of leader peptide binding enables leader-free cyanobactin processing. *Nat Chem Biol* 11:558–563.
11. Ortega MA, et al. (2015) Structure and mechanism of the tRNA-dependent lantibiotic dehydratase NisB. *Nature* 517:509–512.
12. Burkhart BJ, Hudson GA, Dunbar KL, Mitchell DA (2015) A prevalent peptide-binding domain guides ribosomal natural product biosynthesis. *Nat Chem Biol* 11:564–570.
13. Broderick JB, Duffus BR, Duschene KS, Shepard EM (2014) Radical *S*-adenosylmethionine enzymes. *Chem Rev* 114:4229–4317.
14. Frey PA, Booker SJ (2001) Radical mechanisms of S-adenosylmethionine-dependent enzymes. *Adv Protein Chem* 58:1–45.
15. Haft DH, Basu MK (2011) Biological systems discovery in silico: Radical *S*-adenosylmethionine protein families and their target peptides for posttranslational modification. *J Bacteriol* 193:2745–2755.
16. Goldman PJ, Grove TL, Booker SJ, Drennan CL (2013) X-ray analysis of butirosin biosynthetic enzyme BtrN redefines structural motifs for AdoMet radical chemistry. *Proc Natl Acad Sci USA* 110:15949–15954.
17. Goldman PJ, et al. (2013) X-ray structure of an AdoMet radical activase reveals an anaerobic solution for formylglycine posttranslational modification. *Proc Natl Acad Sci USA* 110:8519–8524.
18. Grove TL, Lee K-H, St Clair J, Krebs C, Booker SJ (2008) In vitro characterization of AtsB, a radical SAM formylglycine-generating enzyme that contains three [4Fe-4S] clusters. *Biochemistry* 47:7523–7538.
19. Dowling DP, Vey JL, Croft AK, Drennan CL (2012) Structural diversity in the AdoMet radical enzyme superfamily. *Biochim Biophys Acta* 1824:1178–1195.
20. Hänzelmann P, Schindelin H (2004) Crystal structure of the *S*-adenosylmethionine-dependent enzyme MoaA and its implications for molybdenum cofactor deficiency in humans. *Proc Natl Acad Sci USA* 101:12870–12875.
21. Haft DH (2011) Bioinformatic evidence for a widely distributed, ribosomally produced electron carrier precursor, its maturation proteins, and its nicotinoprotein redox partners. *BMC Genomics* 12:21.
22. Söding J (2005) Protein homology detection by HMM-HMM comparison. *Bioinformatics* 21:951–960.
23. Tsai T-Y, Yang C-Y, Shih H-L, Wang AHJ, Chou S-H (2009) *Xanthomonas campestris* PqqD in the pyrroloquinoline quinone biosynthesis operon adopts a novel saddle-like fold that possibly serves as a PQQ carrier. *Proteins Struct Funct Bioinf* 76:1042–1048.
24. Wecksler SR, et al. (2010) Interaction of PqqE and PqqD in the pyrroloquinoline quinone (PQQ) biosynthetic pathway links PqqD to the radical SAM superfamily. *Chem Commun (Camb)* 46:7031–7033.
25. Latham JA, Iavarone AT, Barr I, Juthani PV, Klinman JP (2015) PqqD is a novel peptide chaperone that forms a ternary complex with the radical *S*-adenosylmethionine protein PqqE in the pyrroloquinoline quinone biosynthetic pathway. *J Biol Chem* 290:12908–12918.
26. Barr I, et al. (2016) The pyrroloquinoline quinone (PQQ) biosynthetic pathway: Demonstration of de novo carbon-carbon cross-linking within the peptide substrate (PqqA) in the presence of the radical SAM enzyme (PqqE) and its peptide chaperone (PqqD). *J Biol Chem* 291:8877–8884.
27. Brennan RG (1993) The winged-helix DNA-binding motif: Another helix-turn-helix takeoff. *Cell* 74:773–776.
28. Li K, Condurso HL, Li G, Ding Y, Bruner SD (2016) Structural basis for precursor protein-directed ribosomal peptide macrocyclization. *Nat Chem Biol* 12:973–979.
29. Hänzelmann P, Schindelin H (2006) Binding of 5′-GTP to the C-terminal FeS cluster of the radical *S*-adenosylmethionine enzyme MoaA provides insights into its mechanism. *Proc Natl Acad Sci USA* 103:6829–6834.
30. Schwalm EL, Grove TL, Booker SJ, Boal AK (2016) Crystallographic capture of a radical *S*-adenosylmethionine enzyme in the act of modifying tRNA. *Science* 352:309–312.
31. Rohac R, et al. (2016) Carbon-sulfur bond-forming reaction catalysed by the radical SAM enzyme HydE. *Nat Chem* 8:491–500.
32. Bruender NA, Bandarian V (2016) SkfB abstracts a hydrogen atom from Cα on SkfA to initiate thioether cross-link formation. *Biochemistry* 55:4131–4134.
33. Shisler KA, Broderick JB (2012) Emerging themes in radical SAM chemistry. *Curr Opin Struct Biol* 22:701–710.
34. Grell TAJ, Goldman PJ, Drennan CL (2015) SPASM and twitch domains in *S*-adenosylmethionine (SAM) radical enzymes. *J Biol Chem* 290:3964–3971.
35. Akiva E, et al. (2014) The structure–function linkage database. *Nucleic Acids Res* 42:D521–D530.
36. Ortega MA, et al. (2016) Structure and tRNA specificity of MibB, a lantibiotic dehydratase from actinobacteria involved in NAI-107 biosynthesis. *Cell Chem Biol* 23:370–380.
37. Regni CA, et al. (2009) How the MccB bacterial ancestor of ubiquitin E1 initiates biosynthesis of the microcin C7 antibiotic. *EMBO J* 28:1953–1964.
38. Moser CC, Anderson JLR, Dutton PL (2010) Guidelines for tunneling in enzymes. *Biochim Biophys Acta* 1797:1573–1586.